Phenotypic plasticity, life cycles, and the evolutionary transition to multicellularity

Si Tang[1]*, Yuriy Pichugin[2,3]*, Katrin Hammerschmidt[1]

[1] Institute of General Microbiology, Kiel University, Kiel, Germany

[2] Department of Evolutionary Theory, Max Planck Institute for Evolutionary Biology, Plön, Germany.

[3] present address: Departament of Ecology and Evolutionary Biology, Princeton University, Princeton NJ, USA.

*These authors contributed equally to this work.

Author ORCIDs
Katrin Hammerschmidt https://orcid.org/0000-0003-0172-8995
Yuriy Pichugin: https://orcid.org/0000-0003-3078-2499

Correspondence and requests for materials should be addressed to KH and YP
katrinhammerschmidt@googlemail.com
pichugin@princeton.edu

Classification
BIOLOGICAL SCIENCES: Evolution

Keywords
cyanobacteria, filaments, phenotypic switch, evolutionary transitions in individuality

SUMMARY

Understanding the evolutionary transition to multicellularity is a key problem in evolutionary biology (1,2). While around 25 independent instances of the evolution of multicellular existence are known across the tree of life (3), the ecological conditions that drive such transformations are not well understood. The first known transition to multicellularity occurred approximately 2.5 billion years ago in cyanobacteria (4–6), and today's cyanobacteria are characterized by an enormous morphological diversity, ranging from single-celled species over simple filamentous to highly differentiated filamentous ones (7,8). While the cyanobacterium *Cyanothece* sp. ATCC 51142 was isolated from the intertidal zone of the U.S. Gulf Coast as a unicellular species (9), we are first to additionally report a phenotypically mixed strategy where multicellular filaments and unicellular stages alternate. We experimentally demonstrate that the facultative multicellular life cycle depends on environmental conditions, such as salinity and population density, and use a theoretical model to explore the process of filament dissolution. While results predict that the observed response can be caused by an excreted compound in the medium, we cannot fully exclude changes in nutrient availability (as in (10,11)). The best fit modeling results demonstrate a nonlinear effect of the compound, which is characteristic for density-dependent sensing systems (12,13). Further, filament fragmentation is predicted to occur by means of connection cleavage rather than by cell death of every alternate cell. The phenotypic switch between the single-celled and multicellular morphology constitutes an environmentally dependent life cycle, which likely represents an important step en route to permanent multicellularity.

RESULTS

To investigate the environmental factors that favor a multicellular morphology, we exposed the single-celled cyanobacterium *Cyanothece* sp. ATCC 51142 (hereafter *Cyanothece* sp.; Figure 1A) to the range of salinities and population densities it would encounter at its isolation site, the intertidal zone of the U.S. Gulf Coast (9). When culturing replicate populations of *Cyanothece sp.* ($5*10^5$ cells/mL) in media with different amounts of added NaCl (0 - 300 mM), we observed that the occurrence of a filamentous morphology after 48 hours (Figure 1A) significantly depends on the salinity of the medium (ANOVA, $F_{10,32}$ = 953.10, P<0.0001). More specifically, at 0 mM NaCl, the whole population displayed a filamentous morphology, ranging from 4-celled up to 16-celled filaments, whereas at 300 mM NaCl (30 PSU), the whole population was single-celled. At intermediate salinities, we always observed both types - 4-celled filaments and single cells - with a higher fraction of filaments up to 90 mM NaCl, whereas at higher salinities single cells represented the most dominant

morphology. Notably we found that populations with a higher fraction of filaments also contain higher cell numbers/mL (ANOVA, $F_{1,32} = 11.658$, P=0.0018).

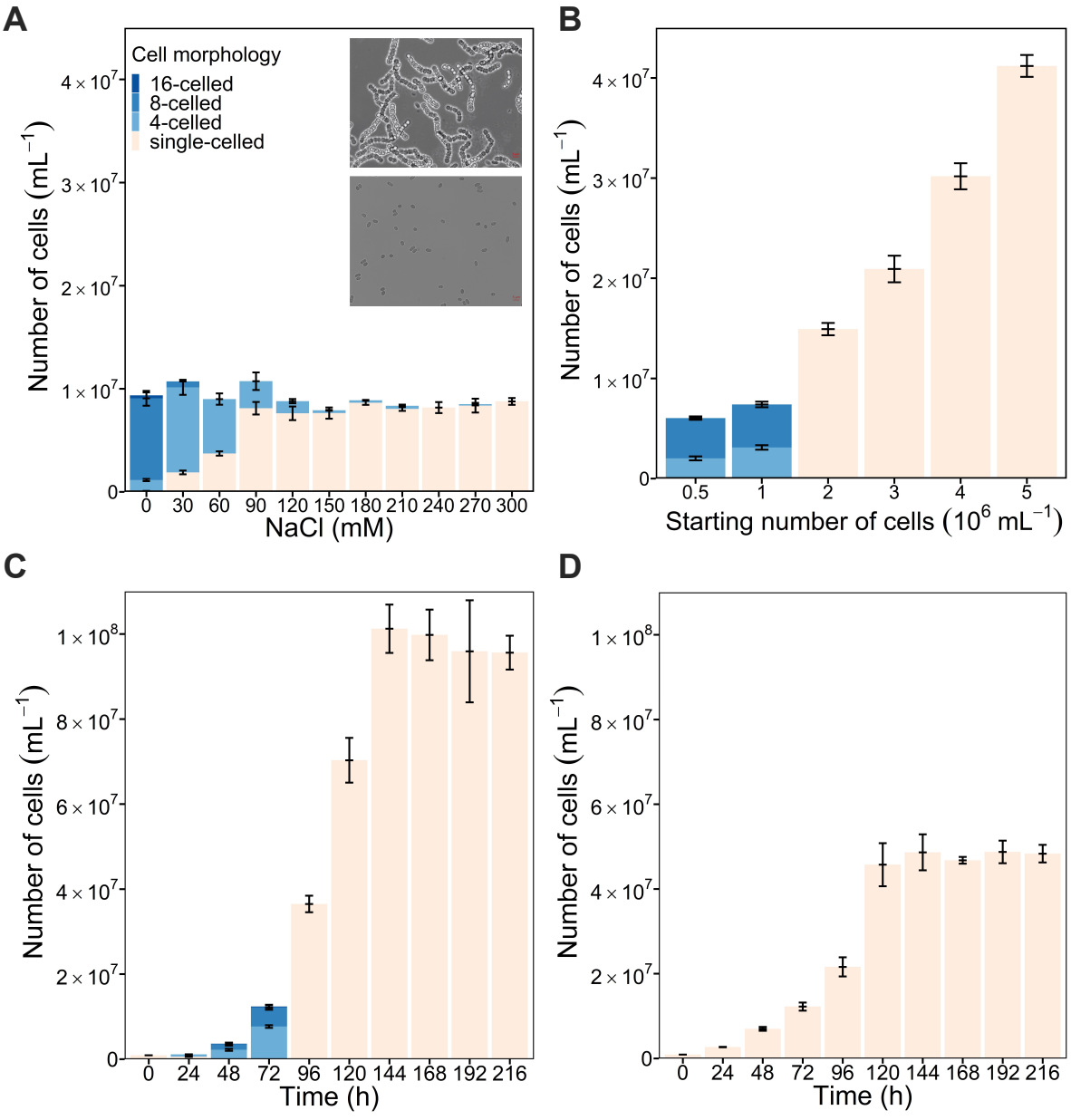

Figure 1 Filamentous morphology of *Cyanothece sp*. ATCC 51142 depends on environmental salinity (at 48h) (A), population density (at 48h; in BG11 without added NaCl) (B), varies over time in batch culture (in BG11 without added NaCl) (C), and is not observed over time in BG11 with added NaCl (300 mM) (D). All experiments were performed in 10 mL media. Error bars represent standard deviation (of each sub-bar for A-C) (n=3).

Next we addressed the role of population density for filament formation (in BG11 media without added NaCl). Replicate populations were initiated with six different starting population densities (all stemming from the same culture), ranging from $5*10^5$ – $5*10^6$ cells/mL. We found that starting cell density was a good predictor of *Cyanothece* sp.'s morphology – after 48 hours we only detected filaments in cultures initiated with low-density,

whereas when initiated with higher starting cell densities (≥2*10^6 cells/mL), we did not observe filaments (Figure 1B, X^2 = 16.89, d.f. = 5, *P* = 0.0047).

To evaluate the effect of population density on population composition in more detail, we followed replicate populations inoculated with single-celled *Cyanothece* sp. of the low-density populations (5*10^5 cells/mL) in 0 mM NaCl media for 5 days (Figure 1C). Already, after 24 hours, we detected first 4-celled filaments. Thereafter, the whole population became filamentous, composed mostly of 4-celled and 8-celled filaments at 48h, and of 4-celled, 8-celled, and 16-celled filaments 72 hours post inoculation. Subsequently, the elongation of the filaments stopped, and from 96 hours post inoculation onwards, we only observed single cells. We found that populations displaying the transient filamentous morphology grew faster and reached higher cell densities as compared to populations that only occur in the single-celled stage throughout their growth cycle (Figure S1; Figure 1D; ANOVA, $F_{1,5}$ = 331.38, *P*<0.0001). Note that the population composition differed depending on the volume of the media; the previously described replicate populations were cultured in 10 mL each. While the same pattern and change between single cells and filaments was observed in volumes of 1 mL each, filaments were present for shorter times so that populations contained single cells already at 72 hours post inoculation (Figure S2).

Cyanobacterial morphology switches are mediated by external cues

The results so far indicate that the observed switches between single cells and filaments and back are density dependent - at higher cell densities, filamentation is inhibited and filament fragmentation is induced. This might be mediated by mechanisms of direct cell-cell contact or through depleted or excreted compounds in the medium. To test this, we harvested both supernatants from cultures inoculated with higher starting cell densities (5*10^6 cells/mL) that did not produce filaments (filament inhibitor; harvested at 24 hours after inoculation, Figure 1B), and supernatants from cultures inoculated with low cell densities (5*10^5 cells/mL) directly after filament fragmentation (filament fragmentor; harvested at 96 h, Figure 1C). To test whether compound (i.e. nutrient) depletion hinders filamentation, we added fresh culture medium (BG11) to both supernatants and to ddH_2O, creating BG11 dilutions from 0 – 100% with 20% increments. Whereas we observed filaments at low media concentrations in ddH_2O (20% BG11, Table S1), we needed to add more BG11 to the two supernatants (60%, 80% BG11) to observe the multicellular morphology. As the lowest nutrient levels are found in the 20% BG11:ddH_2O mixture, where filament formation was observed (in contrast to the 60% and 80% BG11:supernatant mix), an overall depletion of nutrients as the factor hindering filamentation, can be excluded. This notion is supported by the growth trajectory of single cells after fragmentation (Figure 1C), which show that cells can still reproduce (in fact they display the shortest generation time in the period directly after fragmentation, see Figure S1)

and reach a high final concentration in the media post-fragmentation, and so strongly indicates that the post-fragmentation media (i.e. filament fragmentor) contains sufficient nutrients for growth. This can also be seen in the results from the density dependent experiment (Figure 1B), which show that when starting with $5*10^6$ cells/mL, the cell density reached ~ $4.1*10^7$ cells/mL after 48 hours. Note that while we demonstrate that post-fragmentation media contains sufficient nutrients for growth, we cannot fully exclude the depletion of a specific compound required for maintaining growth in the filamentous form.

The harvested supernatants were also added to cultures of low-density single cells and to 48 hours-old filaments and compared to a control, i.e. fresh culture medium (BG11 without the addition of NaCl). After 24 hours of incubation, we observed that both single cells and filaments displayed a different behavior when exposed to the two types of supernatants as compared to the control (Figure 2, ANOVA, $F_{3,35} = 12.25$, $P<0.0001$). While in the control, single cells formed filaments and filaments did not fragment, both supernatants inhibited filament formation from single cells, and also led the filaments to fragment. This strongly suggests that the phenotypic change is not related to direct cell-cell contact, but that substances or the depletion of substances in the supernatant affect the transition between both phenotypes. Interestingly, both supernatants can be used interchangeably – both are able to inhibit filament formation from a single-celled ancestor and are also able to induce filament fragmentation. However, whether both supernatants contain or lack an identical substance needs to be investigated.

As we only observed comparatively short filaments, i.e. with a maximum of 16 cells, before they disintegrated, we investigated whether this is due to culture density (mediated by substances or the lack of substances within the supernatant) or whether it is also modulated by other factors that might constrain filament length. To test this, we diluted cultures containing filaments at 72 h by adding fresh culture media. We found that in diluted cultures, filaments increase in lengths (Figure S3), indicating that the density of the culture affects filament length.

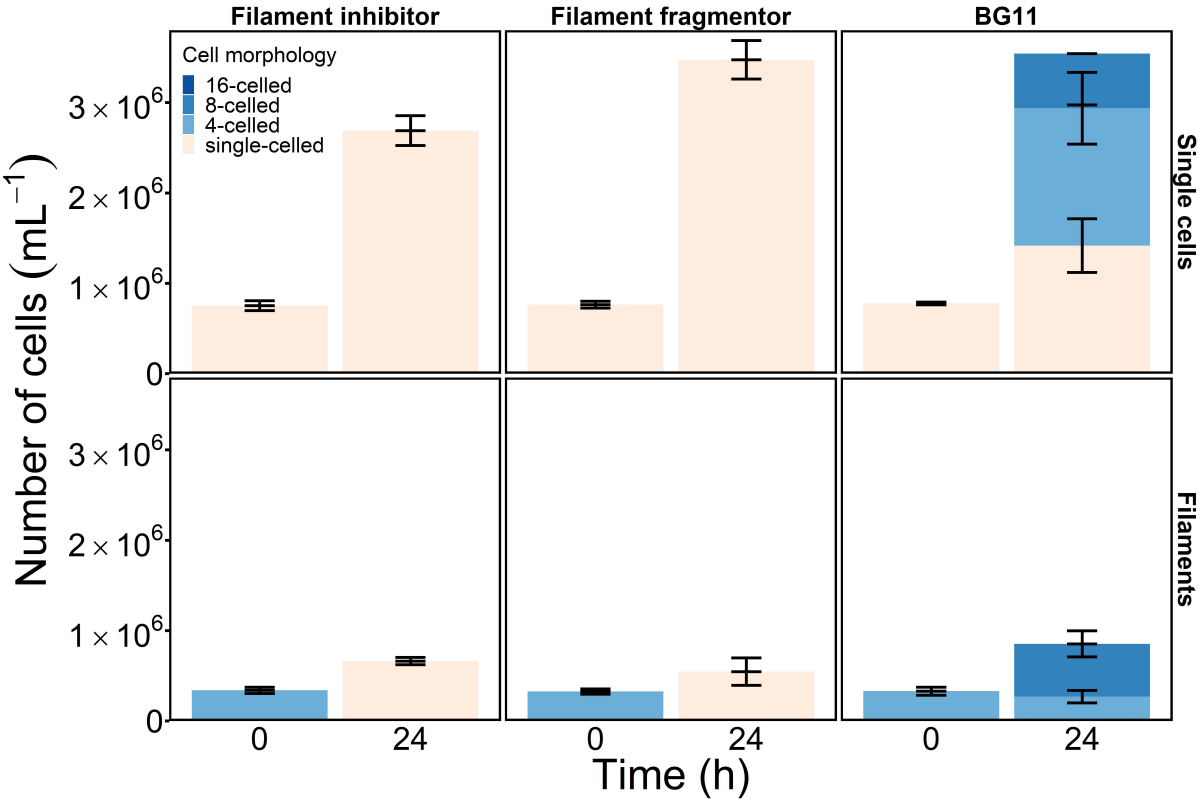

Figure 2 Cell morphology depends on the external medium. Filament inhibitor and fragmentor supernatants stop the formation of filaments from single cells, and lead to the dissolution of existing filaments within 24 hours of exposure. This is in contrast to the control, untreated freshwater medium (BG11), which induces filament formation from single cells and filament elongation. Error bars represent standard deviation of each sub-bar (n=3).

Mechanisms of filament dissolution and compound action

We use the collected data to fit a series of models to compare different hypotheses regarding (i) the mechanism of filament dissolution, i.e. cell death or cleavage of the connection sites, and (ii) the dynamics of the compound, i.e. whether the observed pattern is caused by the accumulation or consumption of a compound. The theoretical modeling approach allows us to explore a much wider set of parameters in different combinations as compared to empirical work.

We consider three families of models. The first family, the *toxic compound models*, assumes that cells produce a compound inducing cell death leading to the fragmentation of filaments. The second family, the *disconnecting compound models*, assumes that cells produce a compound inducing a cleavage of connections between cells. The third family is complimentary to the previous one: these models also assume that filaments fragment due to connections loss, which is caused by a consumption of an initially present compound that stabilizes connections. To highlight this complementarity, this family is referred to as *connecting compound models*. In each family, we consider a number of models, which differ by the character of the compound action (rate of cell death or connection loss) with respect to the compound concentration. For example, we compare individual models, where the

action rate proportionally depends on the concentration, with step-dependence models, where the compound has no effect at concentrations below a certain threshold. In total, we considered 12 models each for the toxic and disconnecting compounds, and 8 models for the connecting compound (see Figures S4, and S5, Tables S2 and S3 for the complete list).

We found that (dis-)connecting models in which fragmentation is caused by the loss of cell connections fit better than the toxic compound models resulting in cell death (Figure 3A). Thus, we conclude that the observed population dynamics is likely a result of cells disconnecting with each other.

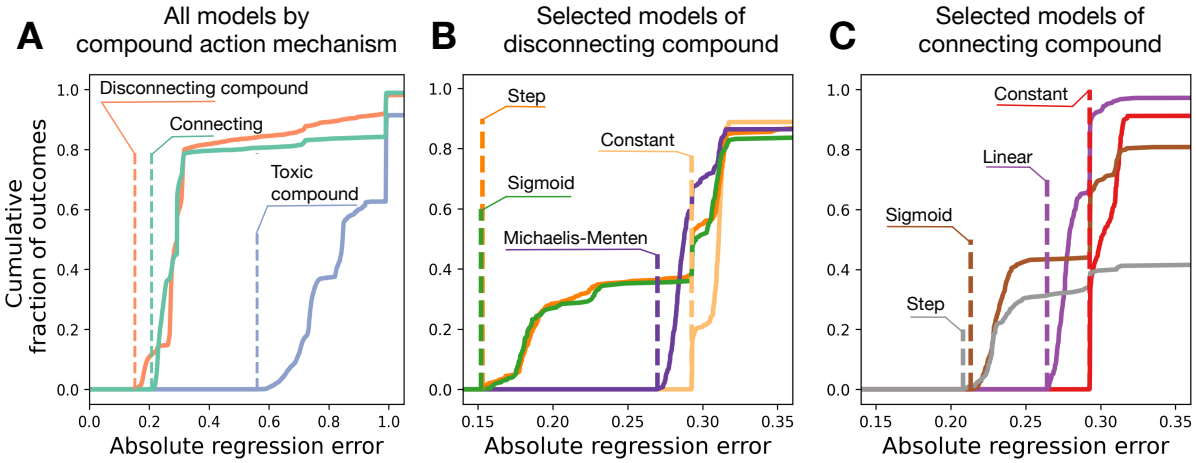

Figure 3 The mechanism of filament dissolution is likely the cleavage of cell connections (A) with a strong non-linear response to active substance concentrations (B, C), as suggested by modeling. Plots show sample cumulative distribution functions of regression errors from 250 independent optimizations for each model. Dashed lines represent the minimal regression error in each group. **(A)** Models in which connections are destroyed due to production (orange, 12 models in total) or consumption (green, 8 models) of a (dis)connecting compound provide much smaller regression errors than models with a toxic compound (blue, 12 models). **(B)** For models with a disconnecting compound (the best class overall), the smallest regression errors were observed among models in which the rate of connection cleavage is negligible at compound concentrations below a certain threshold (e.g. in the step and sigmoid models). **(C)** For models with a connecting compound, the smallest regression errors were observed among models in which the rate of connection cleavage can quickly rise with the compound depletion (e.g. also in the step and sigmoid models). Only four models from each class are shown, for the complete set of models see Figure S6 and Figure S7.

We found that the most accurate fitting is achieved by the disconnecting compound models, where the compound action is near zero when the concentration of the compound is below a threshold: in step and sigmoid models (Figure 3B) and also in fracture, and in breaking point models (Figures S4, S6). There is no significant difference between the regression errors achieved in these four models. The remaining models demonstrate much larger regression errors, similar to those of control models (constant and proportional), see Table S4.

Among the connecting compound models, three out of five best models explicitly feature a threshold (step, sigmoid, and quadratic concave), see (Figure 3C). Two more models with similarly good fit do not have an explicit threshold designed into them (inverse and exponent). Still, all five models share a rapid decrease in filament fragmentation rate at a low compound concentration, followed by a plateau of low sensitivity to concentration – a feature absent among poor fit models (constant, linear, quadratic convex), see Figures S5, S7 and Table S5.

Altogether, connecting and disconnecting models show that in order to observe patterns found in the experiments, the rate of filament fragmentation must depend non-linearly on the compound concentration. In all best fitted models, the fragmentation rate skyrockets at some moment: either after exceeding a threshold compound concentration for the disconnecting compound models, or after expiration of the consumed compound for the connecting models.

DISCUSSION

Phenotypic heterogeneity in microbial populations

When exposing the unicellular cyanobacterium *Cyanothece* sp. ATCC 51142 to a range of salinities comparable to conditions it would experience in its native habitat, the intertidal zone, we observe two distinct microbial lifestyles: the previously described single cell stage (9), and a newly observed filamentous stage (Figure 1A). At low population densities, the single cell stage predominates in cultures with higher salinities (≥90 mM NaCl), while the filamentous stage is most prevalent under low-salinity conditions, and the only stage in the populations cultured in the salinity-free environment. The repeatability and the high rate of the filamentous stage in the population exclude genetic changes, such as mutation or gene amplification (14), as the underlying mechanisms for the change in morphology. Moreover, the co-existence of both morphological stages at the intermediate salinities is indicative of phenotypic heterogeneity.

Phenotypic heterogeneity has been reported for many bacteria and is defined as diverse phenotypes arising from genetically identical microbes that reside in the same microenvironment (15). Several molecular mechanisms underpin phenotypic heterogeneity, such as stochastic state switching, periodic oscillations, cellular age, and cell-to-cell interactions. Whereas in this study, stochastic state switching can be excluded due to the exclusiveness of either of both stages in the two extreme environments (0 mM and 300 mM NaCl), periodic oscillations and cellular age can be excluded when the populations in the different salinities are compared, as all populations were initiated from the same culture. This promotes cell-to-cell interactions as the most likely mechanism underpinning the switch between the two distinct phenotypes. This is confirmed by the outcomes from the experiment, where the effect of starting population density on lifestyle was investigated. Here, the

filamentous stage was only observed at lower population densities (≤1x10^6 mL^{-1}), whereas at higher densities only single cells were observed. This indicates that an increase in cell-to-cell interactions prevents the formation of the filamentous stage. Cell-to-cell interactions could either happen via direct contact between cells (16), or through indirect means, for example in response to cues from other cells that are excreted into the medium, e.g. quorum sensing (17), or through the consumption of nutrients. This was addressed by adding cell-free supernatants from high-density to low-density cultures, which indeed inhibited filament formation, thus confirming that filament inhibition is not caused by direct cell-cell interactions.

Different phenotypic lifestyles are stages of a microbial life cycle

While the different microbial lifestyles and transitions between them have been researched in much detail, this approach only provides a fragmented picture of microbial life cycles that occur in nature (18). When we follow low-density populations of *Cyanothece* sp. in the no-salinity environment over time, a microbial life cycle with alternating single cell and multicellular life stages, can be observed as described for other single-celled bacteria, such as *Bacillus subtilis* that transition through single cell, filamentous, and dormant life stages (18) or for experimental populations of *Pseudomonas fluorescens* (19). In the case of *Cyanothece* sp., 24 hours after initiation of the single-celled culture, filaments can be observed that constitute the only cell-stage for another 48 hours. Thereafter, within the next 24 hours, filaments disappear so that single cells are the only stage present in the population. The disintegration of filaments is an interesting phenomenon, which, as shown for the inhibition of filament formation, depends upon the presence or absence of compounds in the culture medium. Moreover, the two cell-free supernatants can be used interchangeably, i.e. while the filament fragmentor also inhibits filament formation, the filament inhibitor also leads to filament fragmentation.

To learn more about the nature of the compound and about the way filaments transitioned to single cells, i.e. whether every alternate cell dies or whether cells separate through cleavage of connection sites, the experimental data was fitted with 32 different models that vary in the effect of the compound on the filament (cell death or connections cleavage), and in the effect of the concentration of the cue. As the models that assumed cell death resulted in a worse fitting than the ones where the cue resulted in the cleavage of connection sites, filaments likely disintegrate into single cells without cell death.

The classic example for phenotypic switching induced by cues in the medium is quorum sensing (17). The known mechanisms for quorum sensing involve cell-to cell signalling by molecules called autoinducers. They are involved in a regulation pathway featuring a positive feedback loop – the more autoinducer molecules are present, the higher is their production rate (12,13). As a consequence, the kinetic models of quorum sensing feature a bi-stable

dynamics: the cell is either on or off. While the precise kinetics and regulation of the compound lays outside of the scope of our work in the context of this study, the known kinetics models of quorum sensing is best represented by the step model (Figures S4 and S5). The sigmoid model is the generalization of the step model and features it as a limiting case. These two models demonstrate the two best fits in both model families: connecting and disconnecting compound (Tables S4 and S5).

From a theoretical perspective, multicellular life cycles with fission into multiple pieces have a selective advantage when a fragmentation event is costly in some way (20,21). A typical mechanism making fragmentation costly is cell death observed in some species of filamentous cyanobacteria, where specific cells, necridia, undergo programmed cell death, when releasing hormogonia (motile reproductive filaments) from the mother filament (22). The modeling results suggest however that cell death does not happen here. The next alternative is that either production of inhibitor/fragmentor or the response to its high concentration is costly. Given that the results of the fitting indicate a more complex response of *Cyanothece* sp. to inhibitor/fragmentor than the simple mass action law, this supports the hypothesis that some dedicated mechanism, such as quorum sensing, is involved in the observed dissolution of filaments.

Phenotypic plasticity and evolutionary transitions in multicellularity

The environmentally dependent filamentation/fragmentation of *Cyanothece* sp. allows drawing parallels between the population dynamics observed in our study and a life cycle of a multicellular organism. The unicellular phenotype observed in the saline environment is analogous to motile propagules. The process of filamentation in low-salinity conditions represents the growth of the organism. Finally, the fragmentation of filaments into single cells is comparable to reproduction resulting from new propagules being released into nature.

While there is no evidence that the repeated filamentation and fragmentation occurs under natural conditions, we can speculate that the observed effect might be at the core of an environmentally dependent life cycle. Such a hypothetical life cycle would start once single cells of the marine *Cyanothece* sp. find themselves in a compartment with reduced salinity, for example a river estuary. There, through filamentation multicellular chains would be formed until high local densities are reached. Overcrowding would result in the fragmentation of filaments into independent cells. Given the small size of single cells compared to multicellular filaments, the newly released single cells are much more likely to be moved away from the overcrowded environment – either into the sea or to another freshwater compartment, ready to restart the cycle again.

While this is the first report of such an environmentally dependent life cycle for unicellular cyanobacteria, such life cycles are not only known for bacteria, such as *Bacillus subtilis*,

which also alternates between motile single cell and filamentous stages (18). The slime mold *Dictyostelium discoideum*, for example, exists as single cells under favourable conditions, which aggregate into a multicellular slug capable of locomotion upon nutrient depletion (23). Eventually, the slug differentiates into stalk and fruiting body, releasing spores from which new single cells hatch. Another example is the predominantly unicellular marine choanoflagellate *Salpingoeca rosetta*, which forms multicellular colonies In the presence of prey bacteria (24). In all cases, the transition from the unicellular to a multicellular stage is a response to environmental cues. Moreover, even stages of highly sophisticated and integrated developmental animal life cycles have been discovered to depend on external factors and ecological triggers, some of which are based on communication with external bacteria (25). Theoretical models of life cycle evolution have shown that a changing environment can lead to the evolution of complex life cycles in which some cells live and reproduce as unicellular beings, while others form groups (26).

While the transition between the different stages of a life cycle might initially be dependent upon the environment and be based on phenotypic plasticity, recent findings suggest that the integration of these stages likely is central for the evolutionary transition to multicellularity (27,28). One could imagine an ancestral plastic response present in the unicellular ancestor that is co-opted, such as the density dependent switch between single cells and filaments reported here. In that case, the transition from the predominantly unicellular life cycle with facultative multicellular stages to an obligate multicellular life cycle might be straightforward. Given an adequate selective environment, it would simply involve a change from a facultative to an obligate expression of the underlying genes, for example of the ones that are involved in filament formation.

Even though, this life cycle has been artificially induced in the laboratory, it seems to be realistic for what is happening in nature. Many habitats are characterised by rapidly changing environmental conditions, so for example, a unicellular organism isolated in one environment might possess a completely different phenotype/life stage in another. While it is tempting to classify organisms based on their phenotypes, it is important to realise that in the laboratory we often investigate only parts of an organism's life cycle. For studying the transition to multicellularity, the importance of the morphological and physiological flexibility of the unicellular ancestor is becoming more and more apparent, for example when studying the complex life cycles of protozoans (25), which share a common last ancestor with animals or when comparing experimentally evolved nascent stages of early multicellular life cycles to the highly differentiated life cycles and cells of the of their closest multicellular relatives. Thus, at least some (if not all) transitions to differentiated multicellularity might have been a rewiring from temporal differentiation of life cycle stages to spatial differentiation in multicellular organisms (29). This poses important questions regarding the ease of such

342 transitions, the ease of reversals to unicellularity, but also regarding our views of the
343 transition to multicellularity (30). Should we really think about the transition to clonal
344 multicellularity as the multi-step process that starts with the evolution of undifferentiated
345 multicellularity getting more complex over evolutionary timescales or rather as a one-step
346 process starting with a complex unicellular ancestor that directly transitions into a
347 differentiated multicellular organism?

348 **SUPPLEMENTAL INFORMATION**

349 Supplemental information can be found online at . The simulation code, its results, and data
350 processing are publicly available at https://github.com/yuriypichugin/cyanobacteria-filament-
351 fragmentation.

352 **ACKNOWLEDGEMENTS**

353 We thank Peter Deines, Caroline Rose and Nancy Weiland-Bräuer for critical comments on
354 the manuscript. ST was funded by the China Scholarship Council (CSC), Beijing, China. YP
355 is grateful to the Max Planck Society for generous funding. K.H. thanks the Hamburg Institute
356 for Advanced Study (HIAS) and the Joachim Herz Foundation for support.

357

358 **AUTHOR CONTRIBUTIONS**

359 ST and KH designed the experiments. ST performed the experiments. YP performed the
360 theoretical modeling. All authors interpreted the results and wrote the manuscript.

361

362 **DECLARATION OF INTERESTS**

363 The authors declare no competing interests

364 **REFERENCES**

365 1. Maynard Smith, J., Szathmary, E. The Major Transitions in Evolution. Oxford University
366 Press; 1997.

367 2. Szathmary, E. Toward major evolutionary transitions theory 2.0. Proc Natl Acad Sci.
368 2015;112(33):10104–11.

369 3. Bonner, J.T. The origins of multicellularity. Integr Biol Issues News Rev Publ Assoc Soc
370 Integr Comp Biol. 1998;1(1):27–36.

371 4. Schopf, J.W. Microfossils of the Early Archean Apex chert: new evidence of the
372 antiquity of life. Science. 1993;260(5108):640–6.

373 5. Grosberg, R.K., Strathmann, R.R. The evolution of multicellularity: a minor major
374 transition? Annu Rev Ecol Evol Syst. 2007;38:621–54.

375 6. Knoll, A.H. Life on a young planet: the first three billion years of evolution on Earth-
376 updated edition. Vol. 87. Princeton University Press; 2015.

7. Claessen, D., Rozen, D.E., Kuipers, O.P., Sogaard-Andersen, L., Van Wezel, G.P. Bacterial solutions to multicellularity: a tale of biofilms, filaments and fruiting bodies. Nat Rev Microbiol. 2014;12(2):115–24.

8. Herrero, A., Stavans, J., Flores, E. The multicellular nature of filamentous heterocyst-forming cyanobacteria. FEMS Microbiol Rev. 2016;40(6):831–54.

9. Reddy, K.J., Haskell, J.B., Sherman, D.M., Sherman, L.A. Unicellular, aerobic nitrogen-fixing cyanobacteria of the genus Cyanothece. J Bacteriol. 1993;175(5):1284–92.

10. Tuomi, P., Fagerbakke, K.M., Bratbak, G., Heldal, M. Nutritional enrichment of a microbial community: the effects on activity, elemental composition, community structure and virus production. FEMS Microbiol Ecol. 1995;16(2):123–34.

11. Matz, C., Jürgens, K. Interaction of nutrient limitation and protozoan grazing determines the phenotypic structure of a bacterial community. Microb Ecol. 2003;45(4):384–98.

12. Dockery, J.D., Keener, J.P. A mathematical model for quorum sensing in Pseudomonas aeruginosa. Bull Math Biol. 2001;63(1):95–116.

13. Chopp, D.L., Kirisits, M.J., Moran, B., Parsek, M.R. A mathematical model of quorum sensing in a growing bacterial biofilm. J Ind Microbiol Biotechnol. 2002;29(6):339–46.

14. Darmon, E., Leach, D.R.F. Bacterial genome instability. Microbiol Mol Biol Rev. 2014;78(1):1–39.

15. Ackermann, M. A functional perspective on phenotypic heterogeneity in microorganisms. Nat Rev Microbiol. 2015;13(8):497–508.

16. Blango, M.G., Mulvey, M.A. Bacterial landlines: contact-dependent signaling in bacterial populations. Curr Opin Microbiol. 2009;12(2):177–81.

17. Waters, C.M., Bassler, B.L. Quorum sensing: cell-to-cell communication in bacteria. Annu Rev Cell Dev Biol. 2005;21:319–46.

18. van Gestel, J., Ackermann, M., Wagner, A. Microbial life cycles link global modularity in regulation to mosaic evolution. Nat Ecol Evol. 2019;3(8):1184–96.

19. Hammerschmidt, K., Rose, C.J., Kerr, B., Rainey, P.B. Life cycles, fitness decoupling and the evolution of multicellularity. Nature. 2014;515(7525):75–9.

20. Pichugin, Y., Peña, J., Rainey, P.B., Traulsen, A. Fragmentation modes and the evolution of life cycles. PLOS Comput Biol. 2017;13(11):e1005860.

21. Pichugin, Y., Traulsen, A. Evolution of multicellular life cycles under costly fragmentation. PLOS Comput Biol. 2020;16(11):e1008406.

22. Nürnberg, D.J., Mariscal, V., Parker, J., Mastroianni, G., Flores, E., Mullineaux, C.W. Branching and intercellular communication in the Section V cyanobacterium Mastigocladus laminosus, a complex multicellular prokaryote. Mol Microbiol. 2014;91(5):935–49.

23. Bonner, J.T. Cellular slime molds. Princeton University Press; 2015.

24. Fairclough, S.R., Dayel, M.J., King, N. Multicellular development in a choanoflagellate. Curr Biol. 2010;20(20):R875–6.

25. Ros-Rocher, N., Perez-Posada, A., Leger, M.M., Ruiz-Trillo, I. The origin of animals: an ancestral reconstruction of the unicellular-to-multicellular transition. Open Biol. 2021;11(2):200359.

26. Pichugin, Y., Park H. J., Traulsen, A. Evolution of simple multicellular life cycles in dynamic environments. J R Soc Interface. 2019;16(154):20190054.

27. Brunet, T., King, N. The origin of animal multicellularity and cell differentiation. Dev Cell. 2017;43(2):124–40.

28. Staps, M., van Gestel, J., Tarnita, C.E. Emergence of diverse life cycles and life histories at the origin of multicellularity. Nat Ecol Evol. 2019;3(8):1197–205.

29. Bourrat, P., Doulcier, G., Rose, C.J., Rainey, P.B., Hammerschmidt, K. Beyond Fitness Decoupling: Tradeoff-breaking during Evolutionary Transitions in Individuality. bioRxiv. 2021; https://doi.org/10.1101/2021.09.01.458526.

30. Rose, C.J., Hammerschmidt, K. What do we mean by multicellularity? The Evolutionary Transitions Framework provides answers. EcoEvoRxiv. 2021; https://doi.org/10.32942/osf.io/fmw37.

METHOD DETAILS

Bacterial strain and culture conditions

Cyanothece sp. ATCC 51142 was obtained from the ATCC culture collection. Cells were grown photoautotrophically at continuous light with a light intensity of 30 µmol m^{-2} s^{-1} in liquid culture at 30°C. To evaluate the effect of salinity on the morphology of *Cyanothece* sp., we carried out a growth experiment, where we supplemented BG11 media with NaCl. In total, we tested three replicates in each of the eleven NaCl concentrations (0, 30, 60, 90, 120, 150, 180, 210, 240, 270, 300 mM) with a total volume of 10 mL. We recorded the population composition 48 hours after start of the experiment. To test for the effect of starting population density on the morphology of *Cyanothece* sp., we created a gradual series of starting population densities ($5*10^5$, 10^6, $2*10^6$, $3*10^6$, $4*10^6$, $5*10^6$ cells/mL, a total volume of 10 mL), with three replicates per condition. We again recorded the population composition 48 hours after start of the experiment.

Supernatant test

To test whether the phenotypic switch is mediated by nutrient depletion, fresh culture medium (BG11) was diluted with filament inhibitor, filament fragmentor and ddH_2O, creating a gradual series of BG11 ratios (0%, 20%, 40%, 60%, 80%, 100%), within a total volume of 1 mL. Low-density single cells ($5*10^5$ cells/mL) were cultured in all combinations in the 24-well plate, with three replicates for each combination. After 48 hours, the morphology of the cells within each replicate was observed under the microscope and the presence of filaments was recorded.

To investigate whether filament fragmentation depends on cellular age, single cells were grown in 10 mL BG11 in tissue culture flasks for 72 h, after which filament formation was confirmed under the microscope. Cultures were gently mixed, and 20 µL of the filamentous *Cyanothece* sp. population was transferred to 980 µL of fresh BG11 medium. As a control, 1 mL of culture without the addition of fresh medium was grown in parallel. Each treatment was carried out with three replicates. After 24 h, replicate populations (n=3 each) were quantified.

To differentiate whether the morphology changes from single cells to filaments and back have been induced by direct cell-cell contact or through (excreted) compounds in the media, we harvested two supernatants: (i) filament inhibitor, and (ii) filament fragmentor. We created the filament inhibitor supernatant by setting up replicate cultures (n=3) with high starting cell densities ($5*10^6$ cells/mL) in BG11 media. We let them grow for 24 hours under the conditions described above, after which we centrifuged samples (at 20 × g for 3 minutes). Thereafter we processed the supernatant through a 0.22 µm filter (Syringe filter, membrane: PES) to exclude cyanobacterial cells. The process for harvesting the filament fragmentor supernatant was the same, only that the culture was initiated differently. Here, low-density

cultures ($5*10^5$ cells/mL) (n=3) were set up in BG11 and closely monitored. We harvested the supernatant directly after filament fragmentation occurred. Directly after harvesting the supernatants, we set up an experiment, where we exposed replicate populations (n=3 each) of single cells ($5*10^5$ cells/mL) and 48-hours-old filaments to either filament inhibitor or filament fragmentor supernatants or to fresh BG11 media. To achieve this, 1 mL unicellular culture (exponential phase) or 1 mL of 48-hours-old filaments were centrifuged, and the resultant supernatants were discarded. Thereafter cells were resuspended in 1 mL of either filament fragmentor supernatant, filament inhibitor supernatant, or fresh BG11, respectively. We recorded the population composition 24 hours after start of the experiment.

Quantification of population density and composition

Population density and composition was quantified with a cell counting chamber (Neubauer improved, depth: 0.1 mm) from which digital photographs were taken (camera AxioCam MRR3 mounted to the microscope ZEISS Imager.M2m). More specifically, from each replicate population (total volume of 1mL) 1 µL was assayed and cells within the final volume were calculated with the formula: Cells in 1µl = (number of cells in a main square) (1µl) /0.004. Images were counted manually using the software ImageJ, and classified into four categories: single cells, 4-celled filaments, 8-celled filaments and 16-celled filaments.

Statistical analysis

Sample size was chosen to maximise statistical power and ensure sufficient replication. Assumptions of the tests, that is, normality and equal distribution of variances, were visually evaluated. Non-significant interactions were removed from the models. All tests were two-tailed. Effects were considered significant at the level of $P < 0.05$. All statistical analyses were performed with JMP 9. Graphs were produced with R Studio Version 1.4.1564 and Python Matplotlib library.

Theoretical model

In the model, we consider a population composed of filaments of different length. After division, cells always stay together, increasing the length of the filament. Cell divisions in each filament occur synchronously, so the filament length doubles at each division event. However, filaments divide independently from each other, hence division events among different filaments are not synchronized. The rate of cell division in density dependent -- the more cells are present in the population, the slower is cell division:

$$W_{\mathrm{eff}}(\mathbf{x}) = W_0\left(1 - \frac{\sum_i i x_i}{K}\right), \quad (1)$$

where $W_{\mathrm{eff}}(\mathbf{x})$ is the division rate of cells in the population $\mathbf{x}$, W_0 is the maximal division rate, x_i is the number of filaments of the length i, and hence, $\sum_i i x_i$ is the total number of cells in the population, K is the maximal number of cells that can be sustained in the population

(carrying capacity). The maximal possible length of the filament in the model was limited to 32 cells, which is larger than any empirically observed filament. Filaments that reach that maximal size stop dividing.

We assume that filaments fragment due to the changes in the environment caused by the presence of cells. Here we consider three families of models. In **toxic compound** models cells produce a compound causing cell death**.** In **disconnecting compound** models cells produce a compound causing connections cleavage. In **connecting compound** models cells consume a compound that underlies filamentation. In both disconnecting and connecting models, the fragmentation occurs via loss of cell connections but in the first case cells produce the mediating compound, while in the second case they consume it.

In the disconnecting and toxic compound models, cells produce a compound *T*, which causes filament fragmentation. Each cell produces the compound with the unit rate. Produced compound decays with the rate D_{comp}. Hence, the compound dynamics is given by

$$\frac{dT}{dt} = \sum_i i x_i - D_{\mathrm{comp}} T, \tag{2}$$

where the first term describes the production of compound by cells, and the second term describes the compound decay. The rate of compound production is set to one without loss of generality, as it is just a scaling factor for non-observed compound concentration.

In the connecting compound models, a fresh media initially contains a unit concentration of a compound, while cells consume the compound. Hence, the compound dynamics are governed by a different law

$$\frac{dT}{dt} = - D_{\mathrm{cons}} T \sum_i i x_i, \tag{3}$$

where D_{cons} is the rate at which a single cell consumes the compound.

In all cases, population dynamics are described by the set of differential equations

$$\frac{dx_i}{dt} = \sum_j A_{ij}(\mathbf{x}, T)\, x_j, \tag{3}$$

where the projection matrix $A_{ij}(\mathbf{x}, T)$ shows the rate at which filaments of length *i* emerge from the filaments of length *j* by means of growth and fragmentation.

For the connecting and disconnecting compound models, filaments fragment by loosing connections between cells. Hence, the elements of this matrix are

$$A_{ij}(\mathbf{x}, T) = \begin{cases} -W_{\mathrm{eff}}(\mathbf{x}) - (i-1)E(T), & \text{if } i = j \\ W_{\mathrm{eff}}(\mathbf{x}), & \text{if } i = 2j \\ 2E(T), & \text{if } i < j \\ 0, & \text{otherwise} \end{cases} \tag{4}$$

There, the first line describes the disappearance of filaments due to the growth or fragmentation, the second line describes the emergence of twice-longer filaments at each growth event, and the third line describes the emergence of shorter filaments after fragmentation. *E(T)* is the rate of effect of compound at the concentration *T*. In the disconnecting compound models, *E(T)* is a monotonically increasing function – more compound leads to higher rate of connections loss. In the connecting compound models, *E(T)* is a monotonically decreasing function – less compound leads to less stable connections.

For toxic compound models, filaments fragment whenever an internal cell dies. Hence, the elements of this matrix are

$$A_{ij}(\mathbf{x},T)=\begin{cases}-W_{\text{eff}}(\mathbf{x})-iE(T), & \text{if } i=j\\ W_{\text{eff}}(\mathbf{x}), & \text{if } i=2j\\ 2E(T), & \text{if } i<j\\ 0, & \text{otherwise}\end{cases} \tag{5}$$

Note that the only difference between Eqs.(4) and (5) is the coefficient before *E(T)* in the first line. This represents that in a filament of *i* cells, there is *i-1* connections, which can be severed (if the fragmentation is due to the cleavage of connections) but *i* cells that can die (if the fragmentation is due to the death of cells).

For each family, we consider a number of models of the compound effect *E(T)*, see Figures S4 and S5 and Tables S2 and S3. There are 32 models in total. In each family, two control models represent situations, where the mechanism of the compound action is straightforward: the proportional model assumes a mass action law of the interaction between the compound and cells, the constant model assumes a spontaneous fragmentation of filaments, i.e. the compound plays no role. Other models represent situations, where the compound acts on filaments in a more complicated way.

Data fitting and regression results

Four series of experiments are taken into account in the simulations. The first data set is the population composition at different starting densities (Figure 1B). The second data set is the population composition over time (Figure 1C). The third data set is the filament elongation test (Figure S3). The fourth data set is the investigation of the supernatant effects (Figure 2). For each tested combination of parameters, the simulations imitating experimental protocols were conducted.

To simulate the experiment shown in Figure 1B, the population was initialized with solitary cells at given concentrations and the population composition after 48 hours recorded for comparison with experimental observations. To simulate the experiment shown on Figure 1C, the population was initialized with solitary cells at the given concentration and the population

compositions at time points 24, 48, 72, 96, and 120 hours after initialization were recorded. To simulate the experiment shown on Figure 2, first, the population was initialized with high density (filamentation inhibitor), or low density (fragmentation inducer) of solitary cells, and simulated for 24 or 72 hours, respectively. Then, the concentration of the compound was sampled and used in the second simulation series, initialized with populations, given by records at 0 hours in each of the sub-experiments. In each case, the composition after 24 hours was recorded. To simulate the experiment shown in Figure S3, the population was initialized with the record given for 0 hours and the population state after 48 hours was recorded.

In each simulation, the mean square deviation between the experimentally observed and numerically simulated population composition was computed. Minimization of this value by adjusting growth and fragmentation parameters was the target of the fitting.

The experimental data has been fitted with each of 32 numerical models (see Tables S2 and S3 for definitions). The initial values of model parameters have been drawn randomly, so different runs of optimization ended at different points in the parameters space. To compensate for that, 250 independent optimization runs were computed for each model.

Regression errors were scaled by the error provided by the static population. This means that the fitting error provided by the population, which neither grows nor dies and is not affected by the compound, is equal to one. The hypothesis of a static scenario is clearly incorrect; therefore all fitting results with regression errors above one were discarded from the further analysis as completely unrealistic.

All toxic compound models demonstrated much larger regression errors than (dis-) connecting compound models (Figure 3A and Table S4). Among disconnecting models, four models demonstrated similar and low minimal regression errors (0.15 – 0.17): step, sigmoid, fracture, and breaking point. Quadratic model has shown the minimal error around 0.217. The remaining seven models (constant, proportional, linear, top-capped, bottom-capped, Michaelis-Menten, and saturating exponent) resulted in larger errors (0.26 – 0.29), see Figure S6 and Table S4. Among connecting compound models, the lowest regression errors (0.20 – 0.22) were observed for models capable to demonstrate a sudden increase in fragmentation rate at low compound concentrations (step, sigmoid, exponent, inverse, quadratic concave). At the same time, models in which the fragmentation rate increased gradually with compound loss (constant, linear, quadratic convex) resulted in larger regression errors (0.23 – 0.30), see Figure and S7, and Table S5.

Supplemental Information

Phenotypic plasticity, life cycles, and the evolutionary transition to multicellularity

Si Tang, Yuriy Pichugin, and Katrin Hammerschmidt

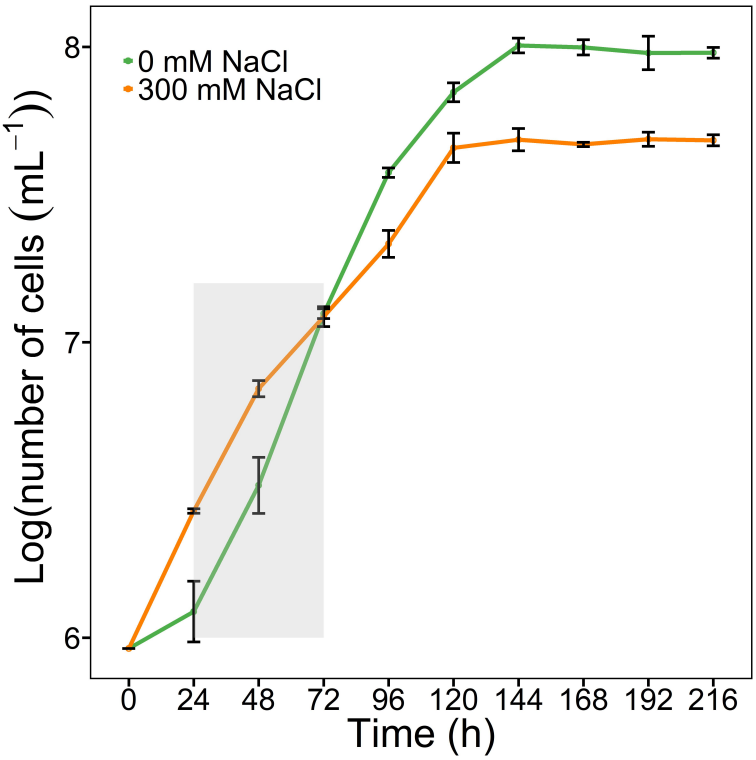

Figure S 1. Comparison of the growth trajectory over time in batch culture in 10 mL BG11 medium with 0 mM and 300 mM NaCl. Grey area indicate the time period when filaments were observed in medium with 0 mM NaCl. The shortest generation time in freshwater is $G_{0\ mM}$ = 15.2 hours (from 72h to 96h), while the shortest generation time in the highest salinity is $G_{300\ mM}$ = 17.5 hours (from 24h to 48h).

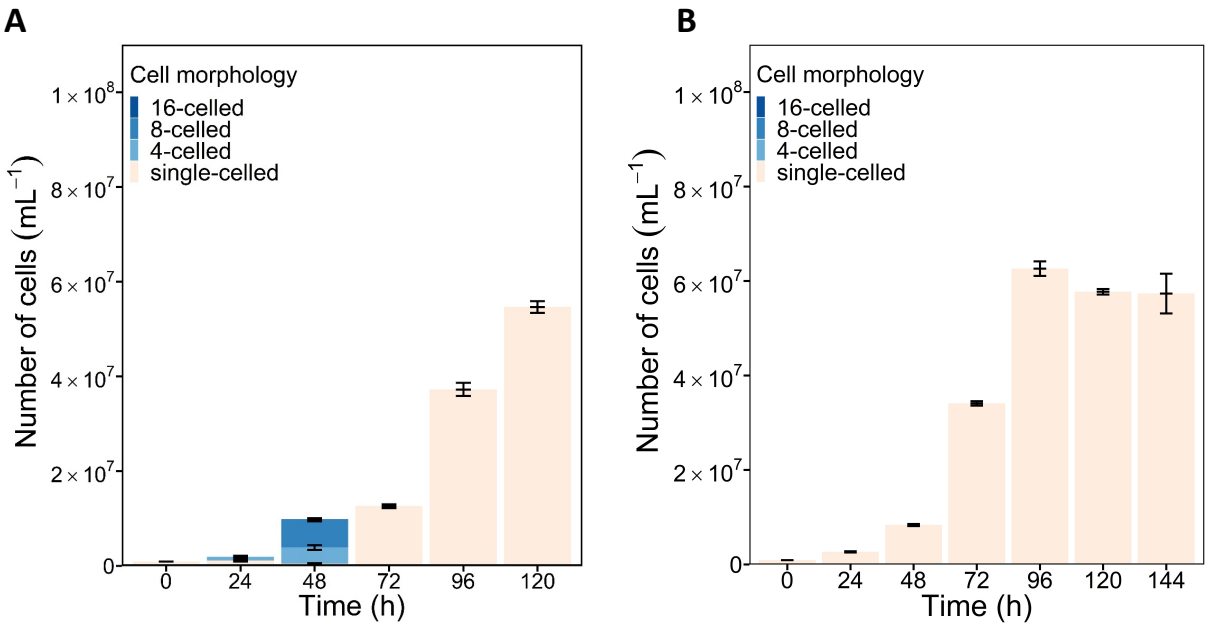

Figure S2. Population dynamics over time in 1 mL volume (24-well plates) in BG11 (A) and in BG11 with 300 mM added NaCl (B).

	BG11 ratio					
	100%	80%	60%	40%	20%	0%
ddH_2O	+	+	+	+	+	-
Filament fragmentor	+	+	+	-	-	-
Filament inhibitor	+	+	-	-	-	-

Table S1. The morphology of *Cyanothece* sp. is dependent on the composition of the medium. Fresh culture medium (BG11) was added to ddH_2O and both supernatants, creating BG11 ratios from 0 – 100% with 20% increments. The emergence of the filamentous morphology was recorded after 48 hours, starting with single cells of *Cyanothece* sp. in each dilution treatment. "+" represents filament occurrence; "-" represents no filament occurrence. While 20% of BG11 in ddH_2O provided sufficient nutrients for filament formation, 60-80% of the BG11 was necessary to dilute the filament fragmentor/inhibitor medium before filaments were observed.

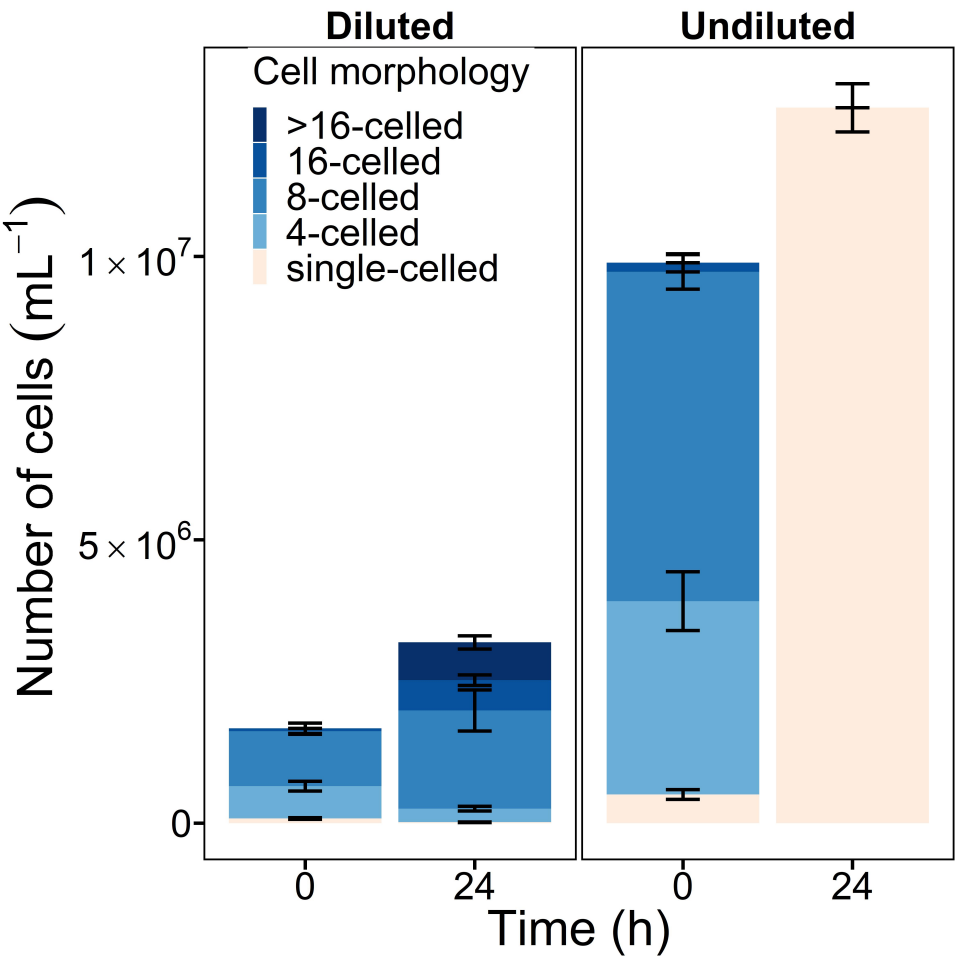

Figure S3. Population composition after the transfer of 72h-old filaments to new medium (left) in contrast to the original population (both in BG11 without added NaCl). When diluted, filaments kept growing and increased in length, indicated by the observation of filaments of longer than 16 cells in length and by a significantly higher proportion of 8-celled filaments, in contrast to the original culture, where 24 hours later only single cells were observed. Error bars represent standard deviation of each sub-bar (n=3).

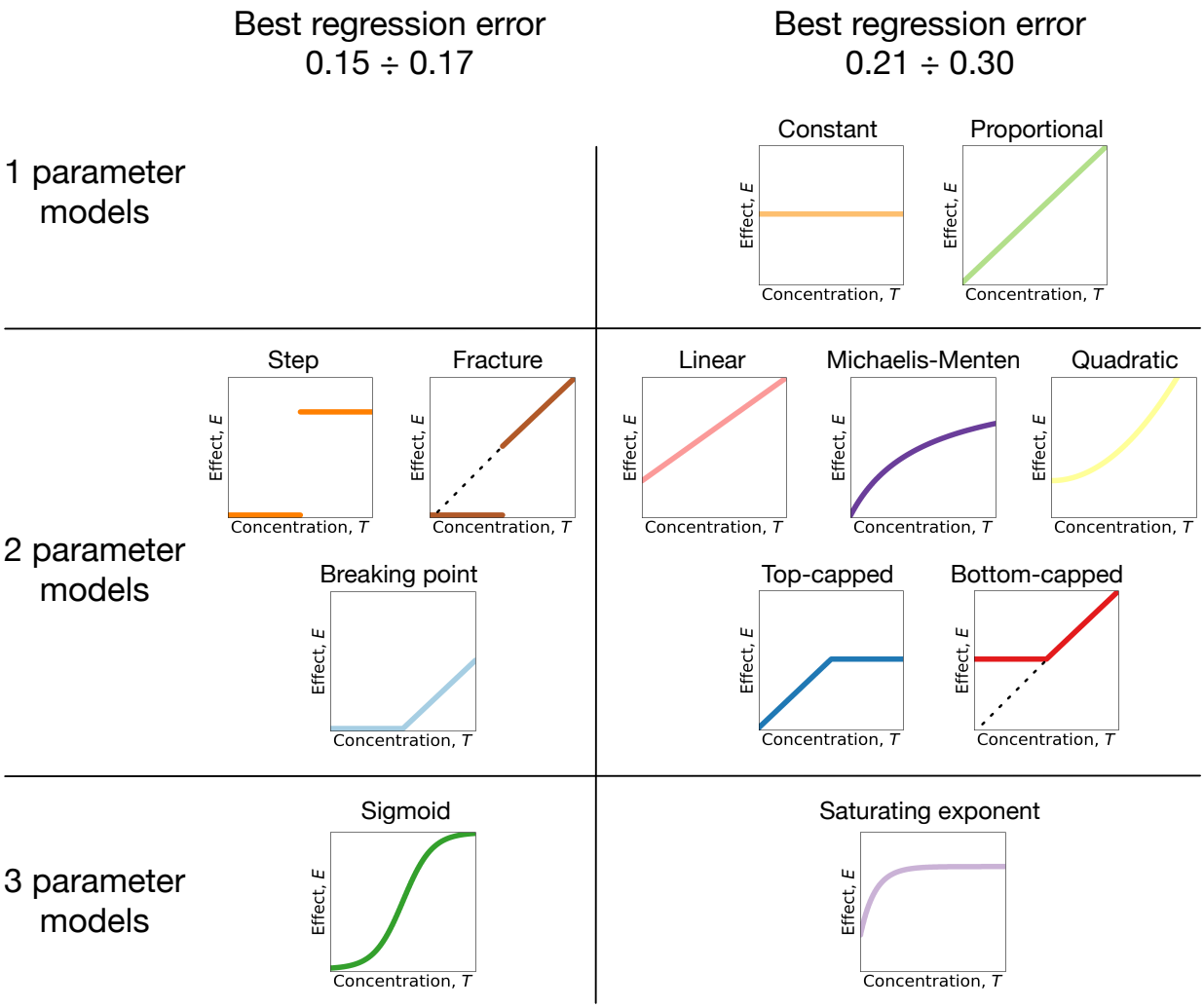

Figure S4. Models of the acting substance concentration effect in the disconnecting and toxic compound models. We consider twelve models of the relationship between acting substance concentration and its effect on the filaments. Two models have a single parameter each and serve as a control. Eight models have two parameters. Two remaining models have three parameters each, see Table S2 for details. Regression errors are shown for the disconnecting compound models. There, four models: step, fracture, breaking point, and sigmoid have shown much smaller regression errors than other models.

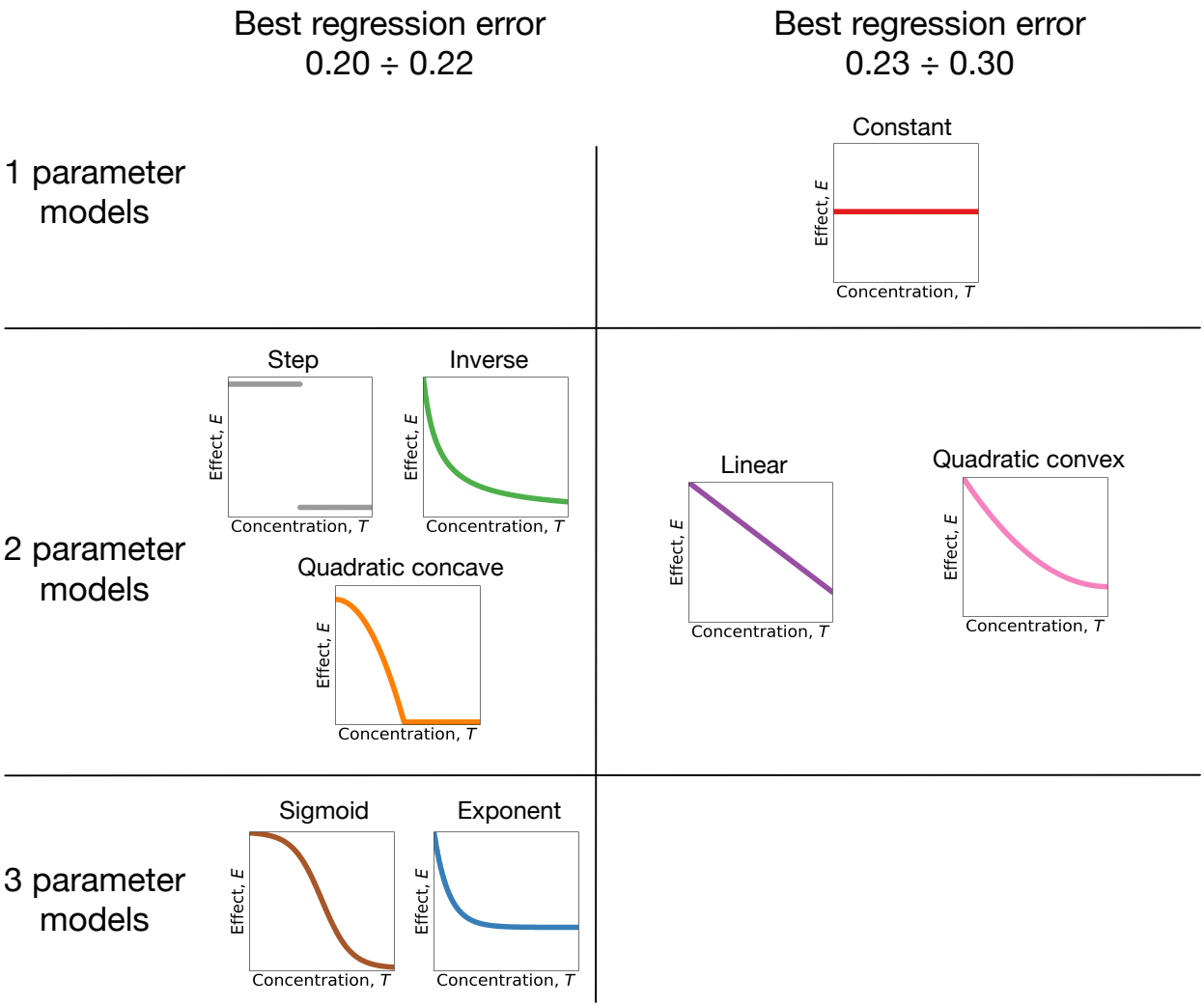

Figure S5. Models of the acting substance concentration effect in the connecting compound models. We consider eight models of the relationship between acting substance concentration and its effect on the filaments. One model has a single parameter and serves as a control. Five models have two parameters. Two remaining models have three parameters each, see Table S3 for details. There, five models: step, inverse, quadratic concave, exponent, and sigmoid have similar small regression errors.

Table S2. Action law E(T) in models used in the toxic and disconnecting compound model families.

Model of the acting substance concentration effect	**Law of action**
1 parameter models	
Constant	$E(T) = E_0$
Proportional	$E(T) = \alpha T$
2 parameter models	
Linear	$E(T) = \alpha T + E_0$
Step	$E(T) = \begin{cases} 0, & T < T_0 \\ E_0, & T > T_0 \end{cases}$
Fracture	$E(T) = \begin{cases} 0, & T < T_0 \\ \alpha T, & T > T_0 \end{cases}$
Breaking point	$E(T) = \begin{cases} 0, & T < T_0 \\ \alpha(T - T_0), & T > T_0 \end{cases}$
Michaelis-Menten	$E(T) = E_0 \frac{T}{T + T_0}$
Quadratic	$E(T) = \left(\frac{T}{T_0}\right)^2 + E_0$
Top-capped	$E(T) = \begin{cases} \alpha T, & T < T_0 \\ \alpha T_0, & T > T_0 \end{cases}$
Bottom-capped	$E(T) = \begin{cases} \alpha T_0, & T < T_0 \\ \alpha T, & T > T_0 \end{cases}$
3 parameter models	
Sigmoid	$E(T) = \frac{E_0}{1 + e^{-\alpha(T - T_0)}}$
Saturating exponent	$E(T) = E_{\max} - (E_{\max} - E_{\min})e^{-\alpha T}$

Table S3. Action law E(T) in models used in the connecting compound models family.

Model of the acting substance concentration effect	**Law of action**
1 parameter models	
Constant	$E(T) = E_0$
2 parameter models	
Linear	$E(T) = \alpha(1 - T) + E_0$
Step	$E(T) = \begin{cases} E_0, & T < T_0 \\ 0, & T > T_0 \end{cases}$
Quadratic convex	$E(T) = E_0 + \alpha(1 - T)^2$
Quadratic concave	$E(T) = max\left(0, E_0 - \alpha T^2\right)$
Inverse	$E(T) = \frac{E_0}{1 + \frac{T}{T_0}}$
3 parameter models	
Sigmoid	$E(T) = \frac{E_0}{1 + e^{\alpha(T - T_0)}}$
Decaying exponent	$E(T) = E_{\max} + (E_{\max} - E_{\min})e^{-\alpha T}$

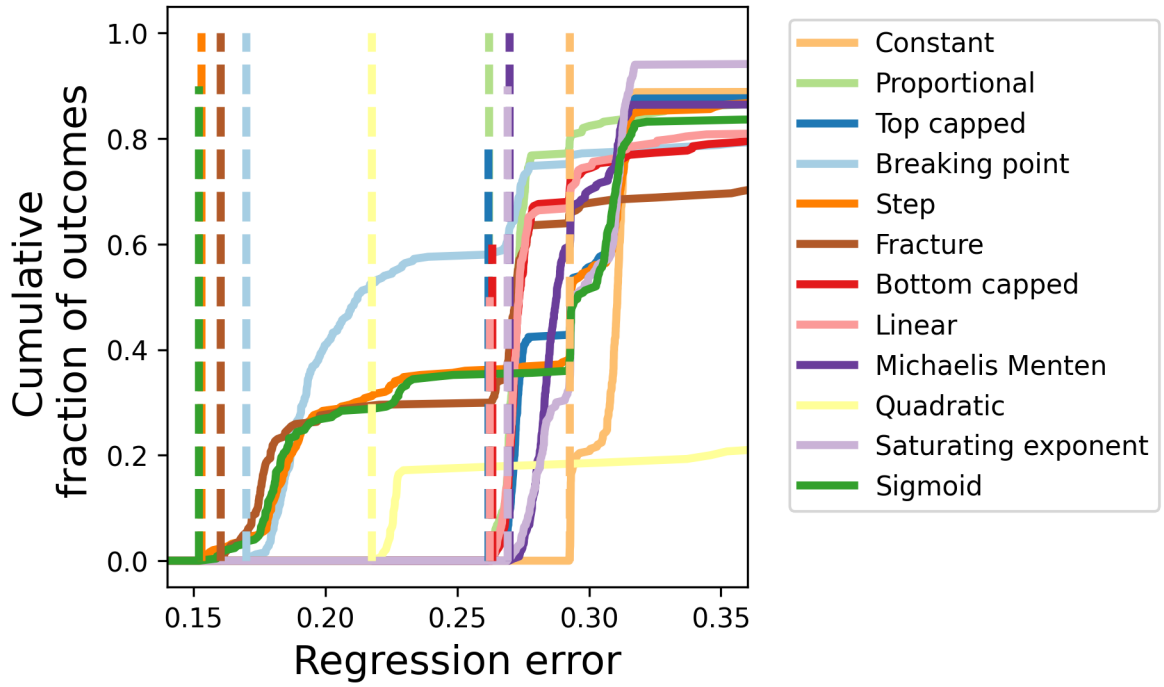

Figure S6. Cumulative distribution functions and the minimal regression errors obtained for each of twelve disconnecting compound models. Studied models can be classified into two groups: models with a good fit having minimal regression errors below 0.17, and models with worse fit, for which the minimal regression error is above 0.21 (can be increased to 0.26 if quadratic model is dropped), see also Table S4. Plots show sample cumulative distribution functions of regression errors from 250 independent optimizations for each model. Dashed lines represent the minimal regression error in each model.

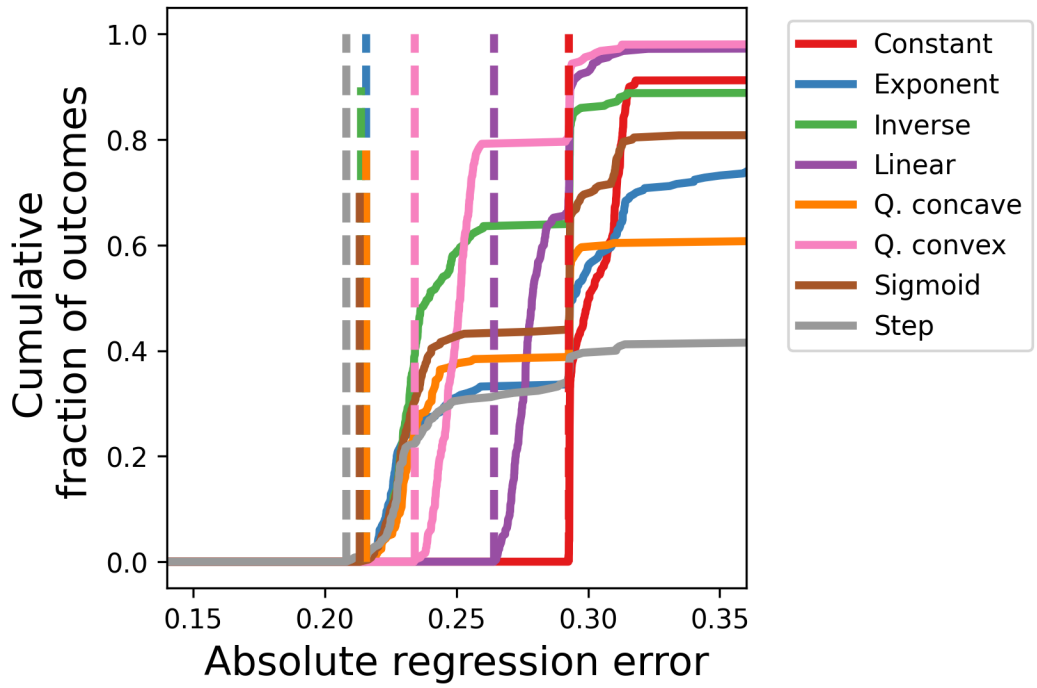

Figure S7. Cumulative distribution functions and the minimal regression errors obtained for each of the eight connecting compound models. Studied models can be classified into two groups: models with a good fit having minimal regression errors around 0.21, and models with worse fits, for which the minimal regression error is above 0.22, see also Table S5. Plots show sample cumulative distribution functions of regression errors from 250 independent optimizations for each model. Dashed lines represent the minimal regression error in each model.

Table S4. Minimal regression errors obtained for the disconnecting and toxic compound models across 250 independent optimizations. Models are sorted by the minimal regression error in the disconnecting compound family. Models with the highest quality fitting are highlighted.

Models	Disconnecting compound regression error	Toxic compound regression error
Sigmoid	0.152	0.583
Step	0.153	0.594
Fracture	0.160	0.721
Breaking point	0.170	0.724
Quadratic	0.217	0.583
Proportional	0.262	0.732
Linear	0.262	0.596
Top-capped	0.262	0.593
Bottom-capped	0.263	0.613
Michaelis-Menten	0.270	0.598
Saturating exponent	0.269	0.560
Constant	0.292	0.590

Table S5. Minimal regression errors obtained for connecting compound models across 250 independent optimizations. Models with the highest quality fitting are highlighted.

Models	**Connecting compound regression error**
Step	0.208
Sigmoid	0.213
Inverse	0.214
Quadratic concave	0.216
Exponent	0.216
Quadratic convex	0.234
Linear	0.264
Constant	0.292

Text S3. Comparison of our study to the cyanobacterial filament fragmentation model by Rossetti et al (2011)

A model of filament fragmentation is also described in Rossetti et al (2011). Their model can be considered as a specific limited case of our set of models. Both our and Rossetti et al models examine growing populations of linear filaments and share the same logistic dependence of the cell division rate from the cell density. However, the model of Rossetti et al includes only filament fragmentation due to cell death, while our model set also includes the mechanism of connection loss.

Another difference between the models is that in our case, cell death is caused by the compound produced by cells; while in the model of Rossetti et al the rate of cell death depends on cell density. In both cases, more cells in a population results in a larger death rate but the model presented here features a reactivity: a sudden increase in cell count does not cause an immediate increase in death rate; instead the death rate will steadily rise with the accumulation of the compound. This difference is of principal importance: the model of Rossetti et al is unable to recover the results of supernatant experiments presented in Fig. 2 – the media plays no role in that model and it is impossible to observe high rates of filaments fragmentation at low cell densities. Nevertheless, the design of the cell death from the model of Rossetti et al can be formally recovered by our models set by choosing the proportional model of compound action (see Table S2 and Fig. S2), plus setting both compound decay rate D_{comp}, and compound toxicity α to very large values. With a high compound decay rate, the equilibration of the compound concentration will occur rapidly, so the death rate will closely follow the cell density. Since a high decay rate also means low overall concentrations of compound, to have any significance, the toxicity must also be high. With this set up our model will behave identically to the model of Rossetti et al, however by doing so, the choice of the compound action mechanism, the model of the compound action, and even the parameter values would be far from optimal.

SUPPLEMENTAL REFERENCES

Rossetti, V., Filippini, M., Svercel, M., Barbour, A.D., Bagheri, H.C. Emergent multicellular life cycles in filamentous bacteria owing to density-dependent population dynamics. J R Soc Interface. 2011;8(65):1772–84.